Analytical Investigation of Pattern Formation in an M-CNN with Locally Active NbO_x Memristors

Ahmet Samil Demirkol*, Alon Ascoli, Ioannis Messaris and Ronald Tetzlaff
Chair of Fundamentals of Electrical Engineering, Technical University of Dresden (TUD), Dresden, Germany
Email*: ahmet_samil.demirkol@tu-dresden.de

2021 IEEE International Symposium on Circuits and Systems (ISCAS) | 978-1-7281-9201-7/20/$31.00 ©2021 IEEE | DOI: 10.1109/ISCAS51556.2021.9401280

***Abstract*—This paper presents the analytical investigation of complex pattern formation in a Memristor Cellular Nonlinear Network (M-CNN) by applying the theory of local activity. The proposed M-CNN has the conventional two dimensional (2D) planar structure, where all the memristive cells are identical and resistively coupled to each other. The single cell is composed of a suitable combination of a DC voltage source, a bias resistor, a locally active NbO_x memristor, and a capacitor. The locally active memristor has a simplified generic form, enhancing the simulation speed, and a functional AC equivalent circuit, facilitating further inspections. The stability analysis of the single cell is followed by the extraction of the parameters of the local activity, edge-of-chaos, and sharp-edge-of-chaos domains. Simulation results demonstrate that pattern formation can emerge in a dissipatively coupled M-CNN with locally active memristors.**

Keywords—Memristor, M-CNN, Local Activity, Pattern Formation, Complexity

I. INTRODUCTION

Spatiotemporal pattern formation, a natural phenomenon that occurs simultaneously in space and time, can be observed in various scientific disciplines [1]. Particularly, it takes place in information processing in biological neural networks and therefore is of special interest in the design of bio-inspired systems. The availability of an analytical design procedure plays an essential role for the realization of pattern formation structures in electrical hardware. In principle, it is possible to generate pattern formation dynamics as a solution to a set of equations, namely reaction-diffusion-partial differential equations (RD-PDEs) [2]. An important hardware structure for implementing locally interconnected dynamical systems and capable to reproduce the spatiotemporal patterns emerging in RD-PDEs are the Cellular Nonlinear Networks (CNNs) [3]. A CNN can be briefly defined as a multi-dimensional homogeneous structure that is composed of locally coupled identical cells. It has already been shown in [4]-[6] that well known spatiotemporal phenomena, such as Turing patterns, auto waves and spiral waves, can be observed in CNNs. The theory of local activity by L. Chua [3], [7] allows to investigate quantitatively the emergence of inhomogeneous solutions in a homogeneous CNN medium. Consequently, on the basis of the theory of local activity, a resistively coupled CNN, that is composed of locally active cells, is capable of generating complex patterns [3], [7].

Motivated from the above discussion, Memristor-CNNs (M-CNNs) [8] have recently appeared as a compact solution for the design of bio-inspired systems, where pattern formation can emerge across a nanoscale hardware platform. Taking into account some noticeable contributions in the literature, locally active memristors have been employed in cell level neural circuit designs [9], [10], while oscillatory dynamics of locally active memristors have been discussed in [11], [12]. The theory of M-CNNs has been comprehensively investigated in [13], [14] and an example for pattern formation in an M-CNN, employing locally active memristors, is introduced in [15], where the coupling among the cells is established via a resistor-capacitor one port.

The aim of this paper is to present the design procedure of a simple M-CNN structure, which can exhibit dynamic pattern formation, while the analytical investigations are conducted by taking into consideration the theory of local activity. The proposed M-CNN has the conventional 2D planar structure, and consists of identical memristive cells which are resistively coupled to each other. The single cell has a compact form and is composed of a DC voltage source, a bias resistor, a locally active NbO_x memristor, and a capacitor. The NbO_x memristor model has a simplified generic form, enhancing the simulation speed, and a functional AC equivalent circuit, facilitating further inspections. We first present the stability analysis of the single cell. We then proceed with the extraction of the parameters of the local activity, edge-of-chaos and sharp-edge-of-chaos domains in terms of the DC operating point of the memristor, of the capacitor, and of the coupling resistor. Lastly, we perform simulations for different values of the design parameters, and successfully show that the proposed resistively coupled M-CNN can generate dynamic patterns.

II. THE LOCALLY ACTIVE DEVICE

For the design of M-CNN cells we utilize the locally active HP NbO_x nanoscale memristor[1] model [16], [17]. The extended form of the original model can be recast into the generic class [18] to enable numerically stable and accurate simulations of the M-CNN structure, reduced in time.

A. Model Equations

The model of the locally active memristor is introduced in (1)-(2), where i_m (v_m) is the memristor current (voltage), R_s is the internal contact resistance, the temperature T is the state variable, $G(T) = g_0 \cdot exp(-g_1/T)$ and $R_{th} = R_{ins}/\left(1+e^{10(T-T_c)}\right) + R_{met}/\left(1+e^{-10(T-T_c)}\right)$ are the temperature dependent memductance and thermal resistance, while the remaining coefficients are model parameters. Note that, for $R_s = 0\Omega$, (1)-(2) specify a core memristor with current $i_{mc} = i_m$ and voltage $v_{mc} = v_m \cdot (1 + R_s \cdot G(T))^{-1}$.

$$i_m = v_m \cdot \frac{G(T)}{1+R_s \cdot G(T)} = v_{mc} \cdot G(T) \tag{1}$$

$$C_{th}\frac{dT}{dt} = \frac{v_m}{1+R_s \cdot G(T)} i_m - \frac{T-T_{amb}}{R_{th}(T)} \tag{2}$$

This work was supported by the German Research Foundation (DFG) under the Project No. 411647366.

[1] The NbOx device, which can be considered as a threshold switch, formally falls into the class of volatile memristors, implied by its memory dynamics as described by the model equations.

978-1-7281-9201-7/21/$31.00 ©2021 IEEE

The DC I-V curve and the S-shaped quasi-static I-V curve under current sweep (with arrows showing the horizontal jumps in the Mott hysteretic region), with and without the contribution of R_s, and the schematic of the memristor, composed of the series combination of the core memristor and R_s, are depicted in Fig. 1(a).

B. The AC Equivalent Circuit

In order to facilitate the upcoming calculations, it is necessary to have the AC equivalent circuit of the memristor. Here we first derive the AC equivalent of the core device and then connect it in series with R_s to obtain the AC equivalent circuit of the overall memristor. For this purpose, the first step is to linearize (1) and (2), i.e. to derive their 1st order Taylor series expansions in the 3 variables, T, v_m and i_m. Taking the Laplace transform of the linearized equations and performing basic algebraic manipulations, one can obtain the 1-port impedance (or equivalently, admittance) function which represents the small-signal response of the memristor at a given equilibrium point. The final form of the AC equivalent circuit of the overall memristor is shown in Fig. 1(b). In the AC equivalent circuit, R_1 corresponds to the inverse of the slope of the DC I-V curve for $R_s = 0\Omega$, and inherently gets negative values in the negative differential resistance (NDR) region. Moreover, the quantity $(R_1 + R_2)$ corresponds to the instantaneous resistance, $V(T_0)/I(T_0)$, of the core memristor at a given temperature T_0 and always gets positive values since the I-V curve lies in the 1st and 3rd quadrant of the I-V plane in all scenarios. The same explanations hold true also for $R_s \neq 0\Omega$ if R_1 is replaced with $R'_1 = R_1 + R_s$. Similarly, L represents the dynamics of the core device and has positive values at all equilibrium points.

III. The Single M-CNN Cell

The proposed M-CNN cell is illustrated in Fig. 2(a), where V_b is a DC voltage source, R_b is a bias resistor, C is a linear capacitor, and the NbO_x memristor is represented as a series combination between the core memristor and the internal contact resistor R_s. Here, one role of the capacitor is to ensure the oscillatory dynamics by increasing the order of the cell, and the other one is to block the DC signal of the associated cell, such that couplings between cells do not disturb the bias conditions.

A. Stability Analysis of the Operating Point

In this section, we present the DC stability analysis of the cell given in Fig. 2(a) in a parametric form, such that it holds true for all equilibrium points. Without sacrificing generality, we will assume that the memristor is biased in the NDR region. Straightforward analysis of the circuit of Fig. 2(a) leads us to (3), which represents the cell state equation.

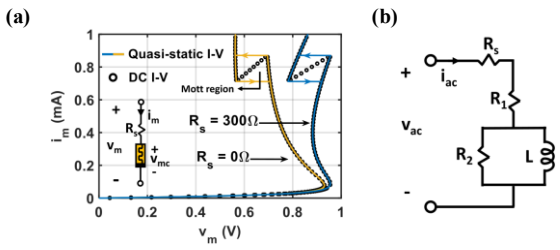

Fig. 1. (a) Quasi-static I-V (solid line) and DC I-V curves (open circle) of the NbO_x memristor. The inset figure shows the schematic of the memristor where the core device and the internal contact resistor R_s are shown separately. The effect of R_s on the I-V curves are depicted through blue ($R_s = 300\Omega$) and yellow ($R_s = 0\Omega$) solid lines. (b) AC equivalent circuit of the NbO_x memristor model where R_s appears in series with the AC equivalent of the core memristor.

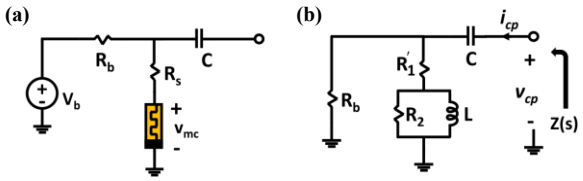

Fig. 2. (a) The cell circuit of the M-CNN structure. V_b is a DC voltage source, R_b is the bias resistor, R_s is the internal contact resistor, C is a DC isolating capacitor, and v_{mc} is the voltage drop across the core memristor. (b) AC equivalent of the circuit in (a), where R'_1 is the series equivalent of R_s and R_1 from Fig. 1(b), i.e., $R'_1 = R_1 + R_s$.

$$C_{th}\frac{dT}{dt} = \left(\frac{V_b}{1+(R_b+R_s)\cdot G(T)}\right)^2 G(T) - \frac{T-T_{amb}}{R_{th}(T)} = f_b(T) \quad (3)$$

The eigenvalue associated with (3) is defined as $\lambda = \frac{df_b}{dT}$ at $T = T_{eqb}$ and is introduced in (4).

$$\lambda = \left[V_b^2 \cdot G'_{eqb} \cdot \frac{1-(R_b+R_s)\cdot G(T_{eqb})}{\left(1+(R_b+R_s)\cdot G(T_{eqb})\right)^3} - \frac{1}{R_{th}(T_{eqb})} + \frac{(T_{eqb}-T_{amb})R'_{th-eq}}{R_{th}^2(T_{eqb})}\right]\frac{1}{C_{th}} \quad (4)$$

Here, both $G'_{eqb} = dG/dT$ and $R'_{th-eqb} = dR_{th}/dT$ are calculated at $T = T_{eqb}$ and the stability condition for the operating point can be stated as $\lambda < 0$. Although (4) appears to be complicated, it is possible to show that the stability condition can simply be expressed as $(R'_1 + R_b) > 0$, taking into account that R'_{th-eqb} is practically zero in the NDR region.

B. Local Activity Analysis

It was shown by Chua in [7] that, in order to establish pattern formation in a resistively coupled homogenous network, the cells of the network have to be locally active. Furthermore, if the equilibrium point of a locally active cell is asymptotically stable, then the cell is said to be at the edge-of-chaos. Moreover, there exists a subset of the parameter space, associated to the edge-of-chaos domain, which includes the parameter values necessary for the destabilization process. This subset of the edge-of-chaos domain is called the sharp-edge-of-chaos domain. Rigorously, a one-port cell is said to be locally active if its small signal transfer function (e.g., $Z(s)$ of Fig. 2(b) for our case), satisfies any of the conditions below:

1. $Z(s)$ has a pole with positive real part, i.e., $Re[s] > 0$.
2. $Z(s)$ has a multiple pole on the *imaginary* ($j\omega$) axis.
3. $Z(s)$ has a simple pole $s = j\omega_p$ on the *imaginary* axis and the *residue* associated to this pole, specifically $r(j\omega) = \lim_{s \to j\omega_p} Z(s)\cdot(s - j\omega_p)$, is either a negative real number, or a complex number.
4. $Re[Z(j\omega)] < 0$ for some $\omega \in (-\infty, \infty)$.

We start applying the theory of local activity by deriving the impedance function $Z(s)$ of the single cell necessarily via its AC equivalent circuit in Fig. 2(b). The resulting impedance function is given parametrically in (5).

$$Z(s) = \frac{s^2LCR_b(R'_1+R_2)+s[L(R'_1+R_2+R_b)+CR'_1R_2R_b]+(R'_1+R_b)R_2}{s^2LC(R'_1+R_2+R_b)+s[CR_2(R'_1+R_b)]} \quad (5)$$

Previously, it was explained that the inequalities $(R_1' + R_2) > 0$ and $(R_1' + R_b) > 0$ should be satisfied. Combining these two pre-conditions, it can be seen from (5) that $Z(s)$ has no poles on the right half plane (RHP). Therefore, the first condition from the above list does not hold true. Similar investigations prove that the second and third conditions are not met either. Thus, $Z(s)$ is stable and therefore, the parameter set where the device is locally active readily coincides with the parameter set where it is at the edge-of-chaos. In order to investigate condition 4 parametrically, we express $Z(s)$ in a compact form as given in (6) where $M_1 = as^2 + c$, $N_1 = b$, $M_2 = ds^2 + f$ and $N_2 = e$.

$$Z(s) = \frac{N(s)}{D(s)} = \frac{as^2+bs+c}{ds^2+es+f} = \frac{M_1+sN_1}{M_2+sN_2}, \tag{6}$$

Extracting the real part of $Z(s)$, it is possible to show that condition 4 translates into a new condition such that $M_1M_2 + \omega^2 N_1N_2 < 0$ for some $\omega \in (-\infty, \infty)$ [19]. This can be further rewritten as $\omega^2(ad) + (be - cd) < 0$ for some $\omega \in [0, \infty)$. Matching (5) and (6), it is easy to show that the final inequality can be satisfied as long as $R_1' < 0$, which is indeed the case for all the equilibrium points in NDR region. As a result, we can conclude that the impedance $Z(s)$ of the cell in Fig. 2(a) is locally active and on the edge-of-chaos at each operating point along the NDR region.

C. Parameter Space Analysis

The above investigations have shown that $N(s)$ and essentially, its parameter b, plays a critical role in satisfying the local activity condition 4, since $D(s)$ prevents all the conditions 1-3 from holding true. Moreover, it is necessary to investigate the roots of $N(s)$ (i.e., the zeros of $Z(s)$), since they take part in the future destabilization process after coupling. As a result, the plots showing the location of the zeros of $Z(s)$ for all the equilibrium points in the NDR region, and for different C values, are given in Fig. 3(a) and in Fig. 3(b) for $R_b = 1k\Omega$, and for $R_b = 5k\Omega$, respectively. Here, LHP zeros lie within the blue (I) region, RHP zeros with complex conjugate values are located in the yellow (II) region, while RHP zeros with purely real values fall into the orange (III) region. Most importantly, the blue regions in Figs. 3(a) and 3(b) contain design parameters under which it is not possible to destabilize the cell via resistive coupling

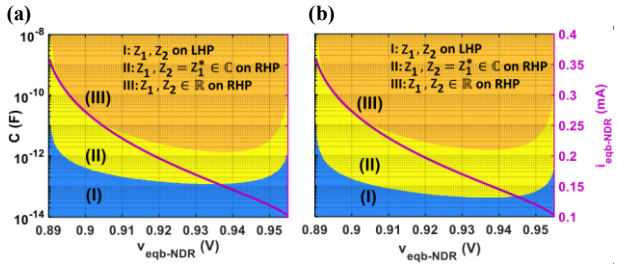

Fig. 3. Location of the 2 zeros z_1 and z_2 of $Z(s)$ on the $v_{m-eqb} - C$ plane for the entire NDR region, with (a) $R_b = 1k\Omega$ and (b) $R_b = 5k\Omega$. The solid purple curve represents the portion of the DC I-V curve in the NDR region. In the blue region (I), both zeros are on the LHP. In the yellow (II) and orange (III) regions, both zeros are on the RHP. The zeros get complex conjugate values in (II) and real values in (III). The regions (II) and (III) contain parameter values, under which the cell may be destabilized via dissipative coupling, due to the existence of RHP zeros within them. Please note that the yellow region gets wider for larger R_b values, which favors the destabilization process.

since all the zeros as well as the poles of the local impedance of the cell itself lie on the LHP in this case. Therefore, the equilibrium point and the C value should be chosen so that the cell would operate either in the yellow II or in the orange III regions of Figs. 3(a) and 3(b). It can be concluded that a larger value of R_b results in a larger yellow (equivalently, a smaller blue) area, which favors the future destabilization of the cell after coupling.

In the following, we would like to investigate the possible stability scenarios after the coupling is established. While an accurate stability analysis would require the investigation of the complete network itself, it would be quite a tedious task, and, therefore, a reasonable simplification is necessary for a quick and qualitative inspection. For this purpose, considering that the type of coupling is defined to be resistive, we assume for the sake of simplicity that a (coupling) resistor is connected between the coupling node (denoted with an open circle) and ground [7], as shown in Fig. 4(a). The stability of the circuit in Fig. 4(a) can be analyzed by examining the poles of the impedance function $Z_c(s)$ of the corresponding AC equivalent circuit in Fig. 4(b). Considering C and R_c as the tunable design parameters, for a given equilibrium point, it is possible to generate a parameter space, which provides information about the location of the 2 poles of $Z_c(s)$. For this purpose, we select a set of equilibrium points (Q1-Q5) along the NDR region, as depicted in Fig. 5(a), and explore the $C - R_c$ parameter space for each of them in Fig. 7(b-f). Here the blue region stands for the domain, where both poles of $Z_c(s)$ fall into the LHP, indicating the stability for the coupled cell. On the other hand, $Z_c(s)$ features 2 RHP zeros with complex conjugate values in the yellow region. Similarly, in the orange region $Z_c(s)$ features 2 RHP zeros with purely-real values. Setting parameters in either the yellow or the orange region result in the instability of the coupled cell. It follows from Fig. 7(b-f) that the overall region, where $Z_c(s)$ has 2 RHP poles, is maximized for Q2 and gets smaller as the equilibrium point shift to either end of the NDR region. Very importantly, the unified unstable region, i.e., the union of the yellow and orange domains, can strictly be considered as the sharp-edge-of-chaos domain, since it is possible to destabilize a cell operating in this region via dissipative coupling.

IV. Pattern Formation

The proposed M-CNN has a 2D grid $(m \times n)$ structure, where m stands for the number of rows, and n stands for the number of columns. $C(i, j)$ represents the cell located at the intersection between the i^{th} row and the j^{th}column of the M-CNN, where $i \in \{1,2, \dots, m\}$ and $j \in \{1,2, \dots, n\}$. Here all the cells are identical, and resistively coupled to the respective nearest neighbors only (assuming open circuit connections

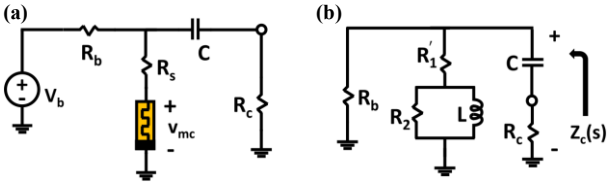

Fig. 4. (a) A simplified scenario for a dissipatively-coupled single cell. Here R_c stands for the coupling resistor. (b) AC equivalent circuit of the cell in (a). The poles of $Z_c(s)$ may be investigated for analyzing the stability of the circuit in (a).

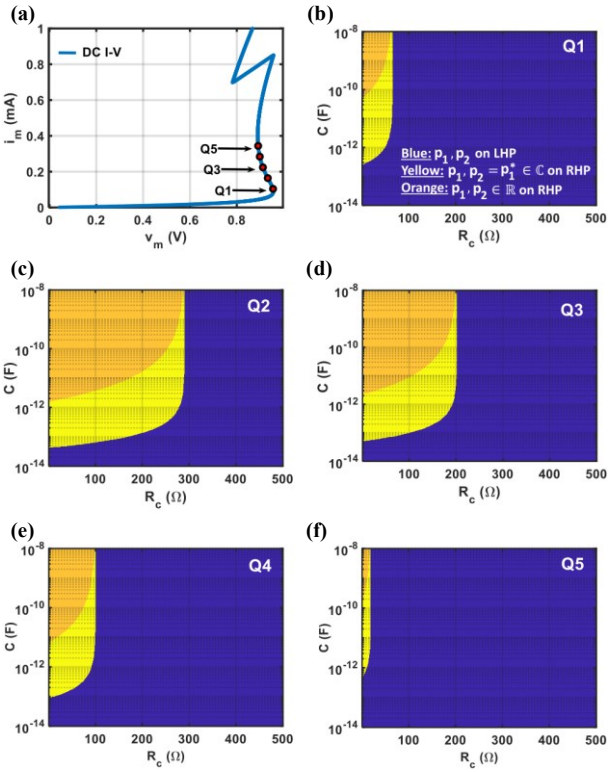

Fig. 5. (a) Location of 5 selected equilibrium points, specifically (Q1-Q5), on the DC I-V curve. (b-f) Qualitative illustration of the stability of the coupled cell on the $R_c - C$ plane for each of the equilibrium points Q1-Q5. In the blue region the two poles p_1 and p_2 of $Z_c(s)$ are on the LHP. In the yellow region $Z_c(s)$ has a pair of complex conjugate RHP poles. Finally, in the orange region, p_1 and p_2 have purely-real values and are located in the RHP. The area of the destabilization region (union of yellow and orange domains) is maximized at Q2. The white legend in (b) is valid also for (c)-(f).

between virtual and boundary cells), as shown in Fig. 6(a). Similarly, the schematic of a single cell, including coupling resistors, is illustrated in Fig. 6(b).

In order to demonstrate pattern formation in the proposed M-CNN, we first simulate a 5×5 $(m = n = 5)$ structure, where we set $R_b = 5k\Omega$, and tune V_b to study the effect of the operating point on the inhomogeneous solutions. Furthermore, we specify the same initial conditions for all the cells, except for $C(3,3)$, so as to trigger the onset of oscillations in the numerical simulations. Fig. 7(a) presents the case where we set V_b to $1.75V$ (which corresponds to the DC operating point Q2 from Fig. 5(a)), R_c to 250Ω and C to $1pF$. For each cell we take 9 regularly-spaced samples in time from the waveform of the memristor voltage across one cycle at steady state, and assign a color hue to each of them

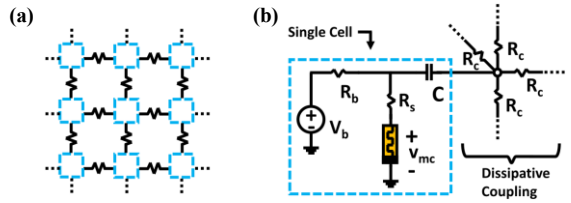

Fig. 6. (a) Resistively coupled 2D grid structure based M-CNN with identical locally coupled cells. (b) Schematic of a single cell, including the network of 4 resistors, each of value R_c, which allows its coupling to the 4 respective nearest neighbors.

according to the coding map on the rightmost part of Fig. 7. The resulting dynamic patterns are shown in Fig. 7(a), where the evolution of cells' dynamics in time may be followed from left to right starting from the 1st row and proceeding down till the 3rd row through the 2nd one. Similarly, Fig. 7(b) illustrates the emergent phenomena for $V_b = 2.2V$. In comparison with the appearance of patterns in Fig. 7(a), the variety in colors is limited in Fig. 7(b), indicating that in the latter case the neighboring cells display a stronger tendency to form phase clusters. Finally, Fig. 8 presents one more example of pattern formation for a large scale M-CNN with $m = 9, n = 25$, where all the cells feature parameter values $V_b = 2.2V$, $R_c = 100\Omega$, and $C = 1pF$, and share the same initial conditions, except for $C(5,13)$. As it may be appreciated from Fig. 8, the network size can affect pattern formation as well.

V. Conclusion

In this work we have presented a resistively coupled M-CNN structure, where each of the identical cells contains a locally-active NbO_x memristor, a DC voltage source along with a resistor for proper biasing, and a linear capacitor. The proposed M-CNN structure is capable of generating different types of dynamic patterns, which shows the attractivity of the proposed design. The context of this work can be extended to the investigation of the impact of variability in parameter values and of the role of initial conditions on pattern formation. Furthermore, future studies will be focused on the development of strategies for the classification of the patterns generated by the proposed M-CNN, and for the realization of the bio-inspired cellular network in hardware.

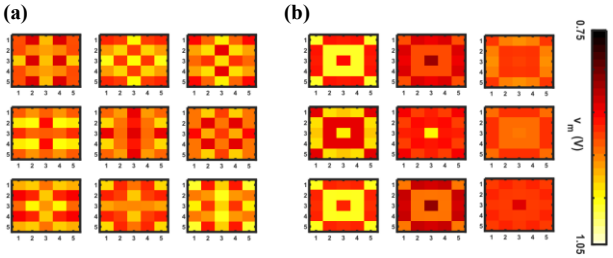

Fig. 7. Simulation results of a $m \times n$ M-CNN structure for $R_c = 250\Omega$, $C = 1pF$, $R_b = 5\text{k}\Omega$, in case V_b is set to 1.75V in (a) and to 2.2V in (b) $(m = 5, n = 5)$. All the cells have the same initial condition except for $C(3,3)$. Shifts in the memristor DC operating point lead to clearly distinct spatiotemporal patterns.

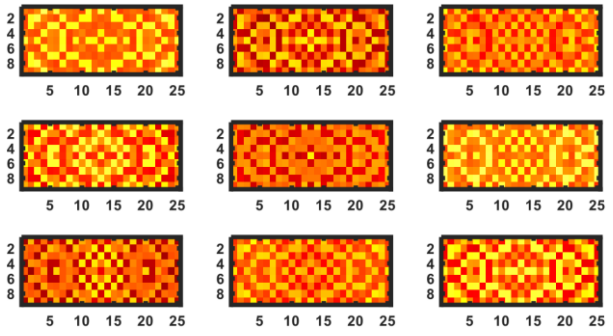

Fig. 8. Simulation results of a large scale $m \times n$ M-CNN structure where $R_c = 100\Omega$, $C = 1pF$, $V_b = 2.2\text{V}$, and $R_b = 5\text{k}\Omega$ $(m = 9, n = 25)$. All the cells have the same initial condition except for $C(5,13)$. Larger M-CNN size results in more intricate patterns.

REFERENCES

[1] D. Walgraef D, “Spatio-Temporal Pattern Formation with Examples from Physics, Chemistry, and Materials Science,” Springer-Verlag New York, NY, 1997. https://doi.org/10.1007/978-1-4612-1850-0.

[2] M. Gilli, T. Roska, L. O. Chua and P. P. Civalleri, "On the relationship between CNNs and PDEs," Proceedings of the 2002 7th IEEE International Workshop on Cellular Neural Networks and Their Applications, Frankfurt, Germany, 2002, pp. 16-24, doi: 10.1109/CNNA.2002.1035030.

[3] L.Chua, “CNN: A Paradigm for Complexity,” World Scientific Series on Nonlinear Science Series A: Volume 31, June 1998. https://doi.org/10.1142/3801.

[4] P. Arena, L. Fortuna and M. Branciforte, "Reaction-diffusion CNN algorithms to generate and control artificial locomotion," in IEEE Transactions on Circuits and Systems I: Fundamental Theory and Applications, vol. 46, no. 2, pp. 253-260, Feb. 1999, doi: 10.1109/81.747195.

[5] B. E. Shi and Tao Luo, "Spatial pattern formation via reaction-diffusion dynamics in 32/spl times/32/spl times/4 CNN chip," in IEEE Transactions on Circuits and Systems I: Regular Papers, vol. 51, no. 5, pp. 939-947, May 2004, doi: 10.1109/TCSI.2004.827628.

[6] A. Buscarino, C. Corradino, L. Fortuna, and M. Frasca, “Turing patterns via pinning control in the simplest memristive cellular nonlinear networks,” in Chaos: An Interdisciplinary Journal of Nonlinear Science, Volume 29, Issue 10, 103145, 2019, https://doi.org/10.1063/1.5115131.

[7] L. Chua, “Local Activity is the Origin of Complexity,” in International Journal of Bifurcation and Chaos, vol. 15, no. 11, pp. 3435-3456, 2005, https://doi.org/10.1142/S0218127405014337.

[8] R. Tetzlaff, A. Ascoli, I. Messaris and L. O. Chua, "Theoretical Foundations of Memristor Cellular Nonlinear Networks: Memcomputing With Bistable-Like Memristors," in IEEE Transactions on Circuits and Systems I: Regular Papers, vol. 67, no. 2, pp. 502-515, Feb. 2020, doi: 10.1109/TCSI.2019.2940909.

[9] M. Pickett, G. Medeiros-Ribeiro and R. S. Williams, ”A scalable neuristor built with Mott memristors,” in Nature Materials, 12, pp. 114–117, 2013, https://doi.org/10.1038/nmat3510.

[10] W. Yi et al., “Biological plausibility and stochasticity in scalable VO2 active memristor neurons,” in Nature communications, 9, 1, 4661, 2018, https://doi.org/10.1038/s41467-018-07052-w.

[11] A. Ascoli, S. Slesazeck, H. Mähne, R. Tetzlaff and T. Mikolajick, "Nonlinear Dynamics of a Locally-Active Memristor," in IEEE Transactions on Circuits and Systems I: Regular Papers, vol. 62, no. 4, pp. 1165-1174, April 2015, doi: 10.1109/TCSI.2015.2413152.

[12] S. Li, X. Liu, S. K. Nandi, D. K. Venkatachalam and R. G. Elliman, “Coupling dynamics of Nb/Nb2O5 relaxation oscillators,” in Nanotechnology, vol. 28, no. 12, 125201, Feb. 2017, doi: 10.1088/1361-6528/aa5de0.

[13] A. Ascoli, I. Messaris, R. Tetzlaff and L. O. Chua, "Theoretical Foundations of Memristor Cellular Nonlinear Networks: Stability Analysis With Dynamic Memristors," in IEEE Transactions on Circuits and Systems I: Regular Papers, vol. 67, no. 4, pp. 1389-1401, April 2020, doi: 10.1109/TCSI.2019.2957813.

[14] A. Ascoli, R. Tetzlaff, S. M. Kang and L. O. Chua, "Theoretical Foundations of Memristor Cellular Nonlinear Networks: A DRM2-Based Method to Design Memcomputers With Dynamic Memristors," in IEEE Transactions on Circuits and Systems I: Regular Papers, vol. 67, no. 8, pp. 2753-2766, Aug. 2020, doi: 10.1109/TCSI.2020.2978460.

[15] M. Weiher, M. Herzig, R. Tetzlaff, A. Ascoli, T. Mikolajick and S. Slesazeck, "Pattern Formation With Locally Active S-Type NbOx Memristors," in IEEE Transactions on Circuits and Systems I: Regular Papers, vol. 66, no. 7, pp. 2627-2638, July 2019, doi: 10.1109/TCSI.2019.2894218.

[16] G. A. Gibson et al., “An accurate locally active memristor model for S-type negative differential resistance in NbOx,” in Applied Physics Letters vol. 108, issue 2, 023505, 2016, doi: 10.1063/1.4939913.

[17] S. Kumar, J. P. Strachan and R. S. Willimans, “Chaotic dynamics in nanoscale NbO2 Mott memristors for analogue computing,” in Nature 548, pp. 318–321, 2017, doi: 10.1038/nature23307

[18] I. Messaris et al., "A Simplified Model for a NbO2 Mott Memristor Physical Realization," 2020 IEEE International Symposium on Circuits and Systems (ISCAS), Sevilla, 2020, pp. 1-5, doi: 10.1109/ISCAS45731.2020.9181036.

[19] F. F. Kuo, “Network Analysis and Synthesis,” Wiley International Edition, John Wiley & Sons, 1964.